

Tunneling anisotropic magnetoresistance of Pb and Bi adatoms and dimers on Mn/W(110): A first-principles study

Soumyajyoti Haldar,* Mara Gutzeit, and Stefan Heinze
*Institute of Theoretical Physics and Astrophysics,
 University of Kiel, Leibnizstrasse 15, 24098 Kiel, Germany*
 (Dated: July 11, 2019)

We show that Pb and Bi adatoms and dimers have a large tunneling anisotropic magnetoresistance (TAMR) of up to 60% when adsorbed on a magnetic transition-metal surface due to strong spin-orbit coupling and the hybridization of $6p$ orbitals with $3d$ states of the magnetic layer. Using density functional theory, we have explored the TAMR effect of Pb and Bi adatoms and dimers adsorbed on a Mn monolayer on W(110). This surface exhibits a noncollinear cycloidal spin spiral ground state with an angle of 173° between neighboring spins which allows to rotate the spin quantization axis of an adatom or dimer quasi-continuously and is ideally suited to explore the angular dependence of TAMR using scanning tunneling microscopy (STM). We find that the induced magnetic moments of Pb and Bi adatoms and dimers are small, however, the spin-polarization of the local density of states (LDOS) is still very large. The TAMR obtained from the anisotropy of the vacuum LDOS is up to 50-60 % for adatoms. For dimers the TAMR depends sensitively on the dimer orientation with respect to the crystallographic directions of the surface due to the formation of bonds between the adatoms with the Mn surface atoms and the symmetry of the spin-orbit coupling induced mixing. Dimers oriented along the spin spiral direction of the Mn monolayer display the largest TAMR of 60 % which is due to hybrid $6p - 3d$ states of the dimers and the Mn layer.

I. INTRODUCTION

The tunneling magnetoresistance (TMR), in which the flow of current depends on the relative magnetization directions of two magnetic layers, has a significant impact on modern day applications ranging from spintronics to magnetic data storage. Using spin-polarized scanning tunneling microscopy (STM), it is even possible to detect the TMR effect for single magnetic adatoms on surfaces¹⁻⁷. The resistance can also depend on the magnetization direction relative to the current direction because of spin-orbit coupling (SOC), which is known as the tunneling anisotropic magnetoresistance (TAMR)^{8,9}. The TAMR is driven by SOC which couples spin and orbital momentum degrees of freedom by the Hamiltonian $H_{SOC} = \xi \mathbf{L} \cdot \mathbf{S}$, where ξ , \mathbf{L} , and \mathbf{S} are the SOC constant, orbital momentum operator and spin operator, respectively. SOC and magnetocrystalline anisotropy effects depend on the environment of an adatom and hence can be tuned by adatom adsorption which have been studied quite extensively¹⁰⁻¹⁴. The TAMR can be observed with only one ferromagnetic electrode and it does not require any coherent spin-dependent transport. Hence, the TAMR is very attractive for spintronics applications^{15,16}. The TAMR was first observed for a double layer of Fe on W(110)⁸. Subsequently, the TAMR has been observed in various systems, e.g., planar ferromagnetic surfaces^{17,18}, tunnel junctions^{9,19-21}, mechanically controlled break junctions^{22,23}. The observed values of TAMR in the above cases are $\approx 10\%$. Attempts have been made to increase the value of TAMR by using $3d$ or $5d$ elements, e.g., using isolated adatoms^{24,25}, bimetallic alloys²⁶ and with antiferromagnetic electrodes²⁷. Recently, Hervé *et al.* have reported a TAMR of up to 30% for Co films on Ru(0001) mediated by surface states²⁸.

Another approach to tune SOC is to use single atoms and dimers of $6p$ elements. The strength of SOC scales with atomic number (Z), principal quantum number (n), and orbital quantum number (l) as $\xi \propto Z^4 n^{-3} l^{-2}$. Hence, $6p$ elements such as Pb and Bi have a higher SOC strength as compared to that of the $3d$ or $5d$ elements studied before. Further tuning of SOC can be achieved by reducing the high rotational symmetry of single atom, i.e., by using dimers of these elements. The effect of strong SOC on unsupported $6p$ dimers has been discussed recently²⁹. In an experimental and theoretical study, Schöneberg *et al.*³⁰ have achieved TAMR values of $\approx 20\%$ by using suitably oriented Pb dimers on the Fe bilayer on W(110) substrate where magnetic domains with out-of-plane magnetization and domain walls with in-plane magnetization can be observed⁸.

In recent years noncollinear magnetic structures at transition-metal interfaces have gained popularity as promising candidates for spintronic applications due to their interesting dynamical and transport properties^{31,32}. A monolayer Mn grown on W(110) surface (Mn/W(110)) is a prominent example which exhibits a noncollinear magnetic structure with a cycloidal 173° spin-spiral ground state along the $[1\bar{1}0]$ direction³³ that is driven by the Dzyaloshinskii-Moriya interaction. Using this magnetic surface with a noncollinear spin structure, it is possible to control the spin direction of adsorbed Co adatoms due to local exchange coupling which has been demonstrated in recent experiments using scanning tunneling microscopy (STM) by Serrate *et al.*^{34,35}. The noncollinear spin state of the Mn monolayer is reflected due to hybridization even in the orbitals of the adsorbed Co adatom³⁶. The possibility of controlling the magnetization direction of an adatom on this surface without the presence of external magnetic field makes this sys-

tem very promising for TAMR studies. Compared to the domain walls of Fe/W(110) used in previous studies³⁰ the spin structure of this surface is known on the atomic scale and allows a quasi continuous rotation of the local spin quantization axis. Recently, Caffrey *et al.* have predicted TAMR values up to 50% for Ir adatoms, i.e. a 5d transition metal, on Mn/W(110)³⁷, however, experimental evidence is missing.

Here we have explored Pb and Bi adatoms and dimers on Mn/W(110) in order to explore the magnitude of TAMR and its dependence on the 6p element and atomic arrangement on the surface. We have used first-principles density functional theory (DFT) calculations to investigate the adsorption of Pb and Bi adatoms and dimers on Mn/W(110) and studied their electronic and magnetic properties. The spin structure of Mn/W(110) is locally well approximated as a two-dimensional antiferromagnet³⁸. We considered two limiting cases of spin directions which are possible due to the cyclodial nature and propagation direction of the spin spiral in the Mn layer: (i) a magnetization direction perpendicular to the surface (out-of-plane) and (ii) a magnetization direction pointing along the $[1\bar{1}0]$ direction (in-plane). Our results indicate that the adsorption of these adatoms facilitates local enhancement of SOC above the surface leading to very large values of the TAMR of 50% to 60% for adatoms. The orientation of Pb and Bi dimers is shown to be crucial in order to achieve even larger TAMR values. This can be understood based on the symmetry of the matrix elements of the SOC Hamiltonian as well as the hybridization of 6p adsorbate with 3d substrate states.

This paper is organized as follows. First, we briefly discuss the computational methods used in our calculations. Then we proceed to discuss the structural, electronic, and magnetic properties, as well as the TAMR of adatoms and the same for dimers in different orientations. The TAMR effects are discussed focusing on the local density of states at the adsorbate atoms and the Mn layer and the vacuum density of states and interpreted based on a simplified model. We summarize our main conclusions in the final section.

II. COMPUTATIONAL DETAILS

In this work we used first-principles calculations using a plane wave based DFT code VASP^{39,40} within the projector augmented wave method (PAW)^{41,42}. For the exchange-correlation, we have used the generalized gradient approximation (GGA) of Perdew-Burke-Ernzerhof (PBE)^{43,44}. For SOC, we followed the methods described by Hobbs *et al.*⁴⁵. We used a 450 eV energy cutoff for the plane wave basis set convergence. Structural relaxations are performed using a $6 \times 6 \times 1$ k-point Monkhorst-Pack mesh⁴⁶. The vacuum local density of states (LDOS) was calculated by placing an empty sphere at a specific height of 5.3 Å above the adatoms onto which the LDOS was

projected. For the calculation of electronic properties, magnetic properties and LDOS, we have used $20 \times 20 \times 1$ k-point Monkhorst-Pack mesh.

A. Structural details

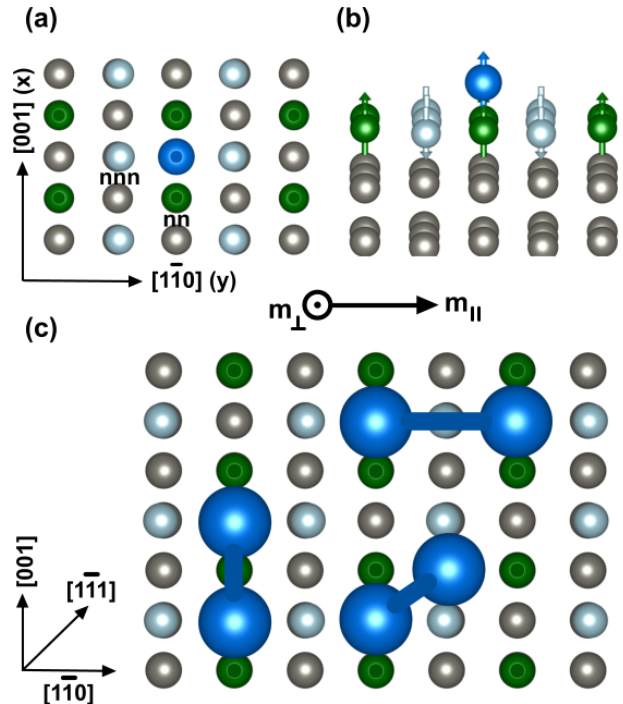


Figure 1. (a) Top view and (b) perspective view of a $c(4 \times 4)$ supercell used for the adatom on Mn/W(110) calculation. Gray spheres represent W atoms while Mn atoms are depicted as green (light blue) spheres with arrows showing the ferromagnetic (antiferromagnetic) magnetic moments with respect to the 6p adatom (dark blue sphere). ‘nn’ and ‘nnn’ are the nearest neighbor and next nearest neighbor Mn atoms to the adatom. x and y refer to the direction of coordinates for the supercell. (c) Top view of a $c(6 \times 6)$ supercell used for dimer adsorption on Mn/W(110) along with the three dimer orientations considered in our calculations. m_{\perp} and m_{\parallel} denote the direction of a perpendicular magnetization and a parallel magnetization with respect to the surface, respectively.

We modeled Mn/W(110) using a symmetric slab consisting of five atomic layers of W with a pseudomorphic Mn layer on each side. We have approximated the local magnetic order of the system as antiferromagnetic, i.e., collinear due to the long periodicity of the spin spiral ground state^{33,34,38}. The effect of the noncollinearity of the spin structure on the electronic states of adatoms has been studied before³⁶. We used a $c(4 \times 4)$ AFM surface unit cell, as shown in Fig. 1(a)-(b). The GGA calculated lattice constant of W, i.e., 3.17 Å is used for our calculations as it is in good agreement with the experimental value of 3.165 Å. A thick vacuum layer of ≈ 25 Å is included in the z direction normal to the surface to

remove interactions between repeating slabs. We added Pb or Bi adatoms at the hollow-site position on each Mn monolayer. The $c(4 \times 4)$ unit cell is large enough to keep the interactions between the periodic images of the adatoms small. For the adsorption of dimers, we have used a larger $c(6 \times 6)$ AFM surface unit cell (see Fig. 1(c)) to keep the interactions coming from the periodic images of the dimers negligible. In the case of Pb or Bi dimers, we have considered three possible dimer orientations on the surface: (i) along the $[001]$ direction, (ii) along the $[1\bar{1}0]$ direction, and (iii) along the $[1\bar{1}1]$ direction as shown in Fig. 1(c). The magnetization direction in calculations including SOC has been chosen normal to the surface, \perp , and along the $[1\bar{1}0]$ in-plane direction, \parallel , as enforced by the cyclodial nature of the underlying spin spiral structure of Mn/W(110)³³. The position of the adatoms, dimers and the Mn layers are relaxed with 0.01 eV/Å force tolerance. We have kept the coordinates of W atoms fixed in all our calculations.

B. Tunneling anisotropic magnetoresistance

Using the spectroscopic mode of an STM, the TAMR can be obtained by measuring the differential conductance (dI/dV) above an adatom or a dimer for two different magnetization directions. The TAMR is obtained from

$$\text{TAMR} = \frac{[(dI/dV)_{\perp} - (dI/dV)_{\parallel}]}{(dI/dV)_{\perp}}, \quad (1)$$

where \perp and \parallel denote a perpendicular magnetization and a parallel magnetization with respect to the surface, respectively. Within the Tersoff-Hamann model^{47,48}, the dI/dV signal is directly proportional to the local density of states (LDOS), $n(z, \epsilon)$, at the tip position in the vacuum, z , a few Ångströms above the surface. Hence, the TAMR can be calculated theoretically from the anisotropy of the LDOS arising due to SOC^{8,24}. Then the TAMR can be calculated as:

$$\text{TAMR} = \frac{n_{\perp}(z, \epsilon) - n_{\parallel}(z, \epsilon)}{n_{\perp}(z, \epsilon)}. \quad (2)$$

III. RESULTS AND DISCUSSION

A. Pb and Bi adatoms on Mn/W(110)

1. Structural and magnetic properties

We begin our discussion with the local structural relaxations upon adsorption of Pb and Bi adatoms on Mn/W(110) which are tabulated in Table I. Our calculations indicate that the hollow site (see Fig. 1(a)) is the most stable adsorption site for both Pb and Bi adatoms. The other sites, e.g., bridge and top sites are unstable for both adatoms in our calculations and collapse to the

Table I. Relaxed distances (in Å) of Pb and Bi adatoms from the Mn atoms of the Mn/W(110) surface. d_{nn} and d_{nnn} denotes the nearest neighbor (nn) and the next-nearest neighbor (nnn) Mn atoms, respectively. Δx , Δy , and Δz are the displacements with respect to the clean surface of Mn atoms after the adsorption of the adatoms. Positive (negative) values imply that the Mn atoms move towards (away from) the adatom.

	d_{nn}	d_{nnn}	Δz_{nn}	Δz_{nnn}	Δx_{nn}	Δy_{nnn}
Pb	2.76	3.17	-0.13	+0.02	-0.01	+0.02
Bi	2.70	2.97	-0.10	+0.06	-0.05	+0.03

hollow site position. The adsorption of the adatoms creates a buckling in the underlying Mn layer in the vicinity of the adsorption sites (see Table I). Significant changes can be observed for the nearest neighbor (nn) Mn atoms, which move away from the adatoms, while the next nearest neighbor (nnn) Mn adatoms move slightly towards the adatoms.

Table II. Magnetic moments (in μ_B) of the adsorbed Pb and Bi adatoms and the nearest neighbor (nn) and next nearest neighbor (nnn) Mn atoms of the Mn monolayer on W(110). For comparison the value of the clean Mn/W(110) surface is given.

	Adatom	Mn _{nn}	Mn _{nnn}	Mn _{clean}
Pb	+0.00	+2.36	-3.34	± 3.41
Bi	+0.08	+2.60	-3.35	± 3.41

The magnetic properties of these systems are affected by the hybridization between the $6p$ adatoms and underlying Mn atoms of Mn monolayer (see Table II). The clean Mn surface of Mn/W(110) have magnetic moments $\pm 3.41 \mu_B$. The p_z orbitals of the adatoms mainly hybridize with the d_{z^2} orbitals of nn Mn adatoms. The magnetic moments of the nn Mn adatoms drop quite significantly for both atom types. They are reduced by 1.05 μ_B and 0.81 μ_B for Pb and Bi adsorption, respectively. Due to the hybridization, the induced magnetic moment on Bi adatom is 0.08 μ_B , whereas the Pb adatom is non-magnetic.

The effect of hybridization is less prominent for the nnn Mn adatoms where a slight reduction of magnetic moment $\sim 0.06 \mu_B$ occurs for both adatoms.

2. Electronic properties

Next, we discuss the electronic properties of the $6p$ adatoms adsorbed on the Mn/W(110) surface. Fig. 2 shows the spin-resolved LDOS of the Pb and Bi adatom adsorbed on Mn/W(110), the LDOS of the neighboring Mn atoms, and m_l decomposed p states of Pb and Bi adatom. These calculations have been performed in the scalar relativistic approximation, i.e., neglecting SOC.

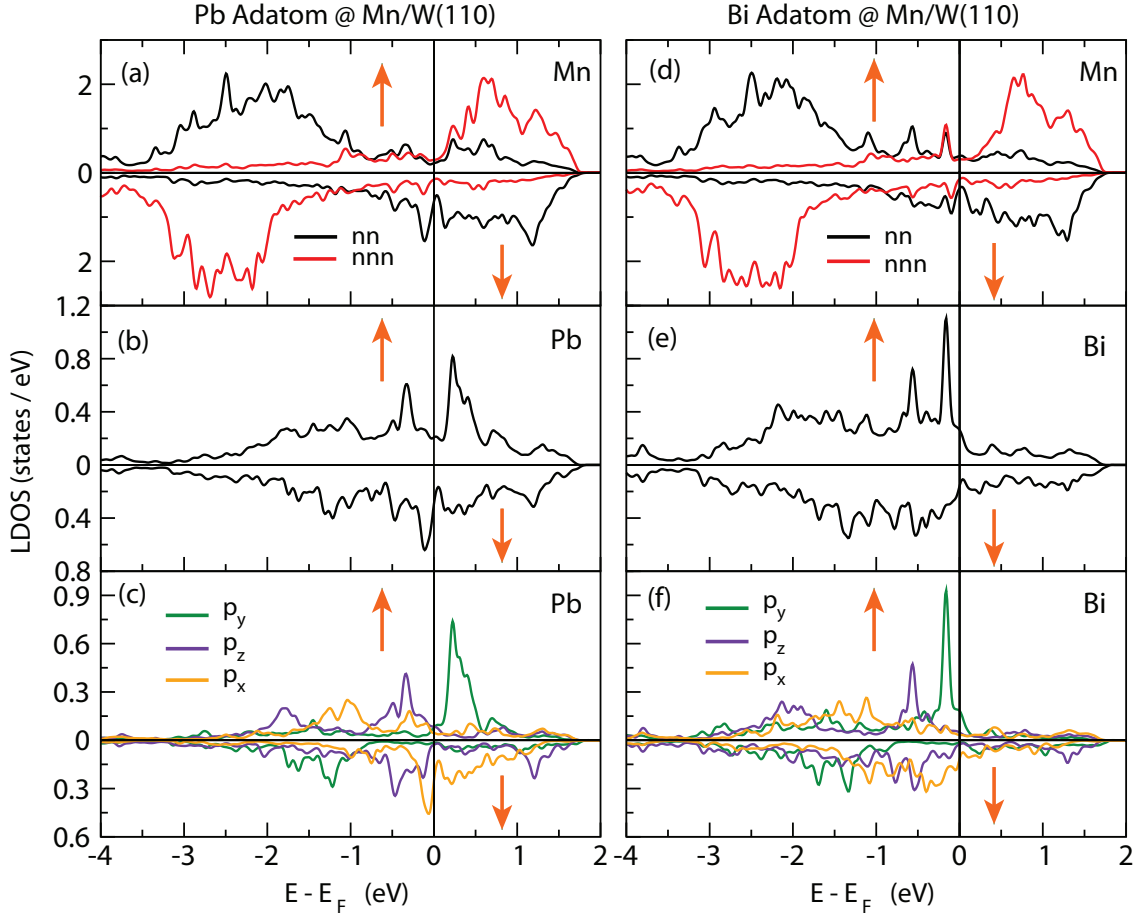


Figure 2. (a, d) Scalar relativistic spin-resolved LDOS of the neighboring (nearest ‘nn’ and next-nearest ‘nnn’) Mn atoms of the Pb and Bi adatom adsorbed on Mn/W(110). (b, e) Scalar relativistic spin-resolved LDOS of the Pb and Bi adatom. (c, f) Scalar relativistic m_l decomposed spin-resolved LDOS for Pb and Bi adatom. Majority and minority states respectively are defined with respect to the nearest neighbor Mn atoms of the Mn monolayer. The orange up and down arrow indicates majority and minority spin channels, respectively.

A possible hybridization can be observed by calculating and comparing the spin-resolved LDOS of the adatoms with the neighboring Mn states as shown in Fig. 2. This hybridization effect is clearly observed just below E_F where minority Mn peaks are located at the same position as p_x and p_z states of the adatoms. Further interactions are observed for Pb around $E_F - 0.50$ eV, $E_F - 0.34$ eV, where the states from the adatoms interact with the states from the nn Mn atoms. In this energy range one also sees reduced exchange splitting of the nn Mn states as compared to the nnn Mn states which affects the magnetic moment of the nn Mn atoms as mentioned in section III A 1. The magnetic moment of nn Mn atoms drops to $2.36 \mu_B$ and $2.6 \mu_B$ upon adsorption of the Pb and Bi adatom, respectively. Despite the small spin splitting observed for both adatoms, the spin polarization of the adatoms is quite large. The spin polarization of the adatoms varies in-between $\pm 40\%$ which is mainly arising from the p_z and p_y states of the adatoms.

Previously, it has been shown that the spin direction

of adsorbed Co adatoms on Mn/W(110) can be detected in spin-polarized STM images at small bias voltages due to the different orbital symmetry of d states in majority and minority spin channel³⁴. We find a similar effect for the p orbitals of Pb close to the Fermi energy, E_F . Figure 3 shows top and cross-sectional spin-resolved partial charge density plots in a small energy window [$E_F - 0.065$, $E_F - 0.045$ eV] for Pb adatom adsorbed on Mn/W(110). A strong interaction between the minority p_x states of the adatom and the minority d_{z^2} orbitals of the neighboring Mn atoms is clearly visible in the cross-sectional plot along the [001] direction shown in Figs. 3(d). Here, the axes of the d_{z^2} Mn orbitals are distorted pointing towards the Pb atom and a large part of the charge density is concentrated at the interface between adsorbate and substrate. However, such hybridization is less prominent in the majority channel which displays the rotationally symmetric shape of a p_z orbital [Fig. 3(c)].

The partial charge density calculated at a height of 3 Å in the vacuum [Fig. 3(a-b)] shows that the both spin

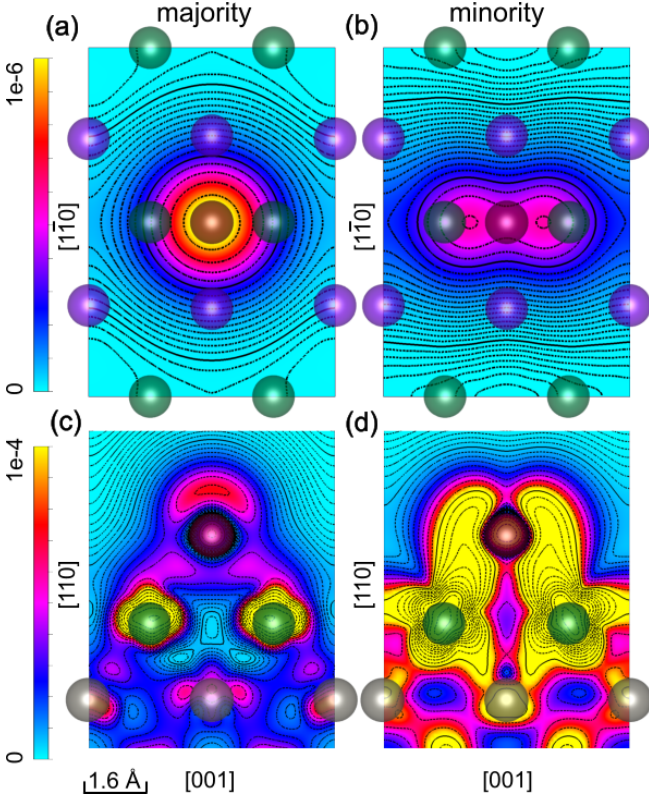


Figure 3. (a, b) Spin-resolved partial charge density plots at 3 Å above the Pb adatom on Mn/W(110) in the energy range $[E_F - 0.065, E_F - 0.045 \text{ eV}]$. (c, d) cross-sectional plots through the Pb adatom parallel to the $[001]$ direction for the charge densities of the top panel.

channels are clearly distinguishable from each other due to the shape of their orbitals. For the majority channel one can clearly observe the p_z states of the adatom in the vacuum. In the minority channel, the double-lobed structure of the p_x state protrudes rotationally symmetric states such as s , p_z and d_{z^2} orbitals which usually extend further into the vacuum. Similar behavior has been reported previously by Serrate *et al.* for different d -states of a Co adatom adsorbed on Mn/W(110)³⁴. Hence, we can conclude that in an STM experiment with a magnetic tip it will be possible to identify the spin direction of the Pb adatom by means of the respective orbitals dominating near E_F yielding similar effects observed in spin-polarized STM^{34–36}.

However, for the Bi adatom the above mentioned feature is not present in the vicinity of E_F which is accessible for STM. In this case, the majority p_y states of Bi are completely covered by the rotationally symmetric orbitals in the vacuum (not shown). Therefore, the orbital shapes for majority and minority states for the charge densities calculated in the vicinity of E_F do not differ from one another.

3. TAMR of Pb and Bi adatoms on Mn/W(110)

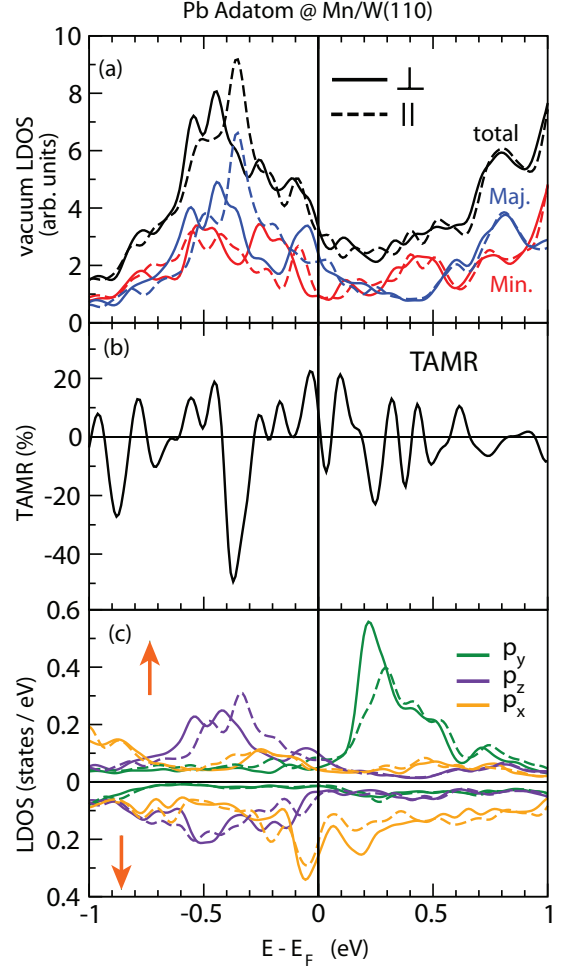


Figure 4. (a) Total (black lines) and spin-resolved (Majority: blue, Minority: red) vacuum LDOS including SOC above the Pb adatom on Mn/W(110) for out-of-plane (\perp , solid lines) and in-plane (parallel to the $[1\bar{1}0]$ direction) magnetizations (\parallel , dashed lines). (b) TAMR obtained from the spin-averaged vacuum LDOS according to Eq. (2). (c) Orbital decomposition of the LDOS of the Pb adatom in terms of the majority (up) and minority (down) states. Solid (dashed) lines correspond to the magnetization direction perpendicular (parallel) to the surface plane. The orange up and down arrow indicates majority and minority spin channels, respectively.

In this section we will focus on the description of the electronic structure of $6p$ adatoms adsorbed on the Mn monolayer of W(110). Especially the anisotropy of the LDOS due to SOC and the subsequent TAMR effect will be discussed in detail.

Fig. 4(a) shows both the total (spin-averaged) and spin-resolved vacuum LDOS above the Pb adatom – in an energy range around E_F typically accessible to STM – calculated for the two magnetization directions including SOC: (i) perpendicular to the surface (out-of-plane) denoted as $n_\perp(z, \epsilon)$ and parallel to the $[1\bar{1}0]$ direction

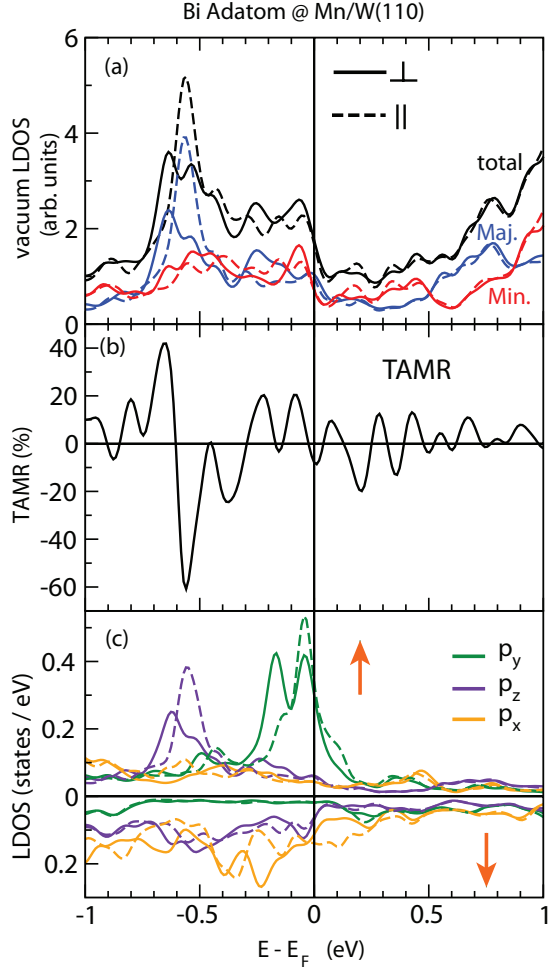


Figure 5. (a) Total (black lines) and spin-resolved (Majority: blue, Minority: red) vacuum LDOS including SOC above the Bi adatom on Mn/W(110) for out-of-plane (\perp , solid lines) and in-plane (parallel to the $[1\bar{1}0]$ direction) magnetizations (\parallel , dashed lines). (b) TMR obtained from the spin-averaged vacuum LDOS according to Eq. (2). (c) Orbital decomposition of the LDOS of the Bi adatom in terms of the majority (up) and minority (down) states. Solid (dashed) lines correspond to the magnetization direction perpendicular (parallel) to the surface plane. The orange up and down arrow indicates majority and minority spin channels, respectively.

(in-plane) denoted as $n_{\parallel}(z, \epsilon)$. Differences between both magnetization components are clearly discernible in the energy range below the Fermi level (E_F). The most significant feature is located at -0.37 eV in $n_{\parallel}(z, \epsilon)$ and corresponds to a peak of majority p_z states being split and shifted towards lower energies as the magnetization rotates from the film plane (\parallel) to the perpendicular (\perp) direction of the surface. The same effect, although much less prominent, is also visible for the minority states. This behavior leads to a maximum value in the TMR of -49% (see Fig. 4(b)). Around E_F this effect is considerably smaller and of opposite sign with TMR values up to $+22\%$.

Similar observations can be seen in the vacuum LDOS of the Bi adatom on Mn/W(110) shown in Fig. 5(a). Here, the dominant peak of majority p_z states which splits likewise upon rotation of the magnetization direction is shifted by 0.2 eV towards lower energies compared to Pb. Linked to this state, the value of the TMR first takes a local maximum of $+42\%$ at -0.66 eV before dropping abruptly to a minimum of -61% at -0.57 eV below E_F . Similar to Pb, differences concerning n_{\perp} and n_{\parallel} for the minority channel are small in this energy range and the main part of the TMR originates from majority states. In contrast, states with minority character are causing a modest TMR of $+20\%$ just below E_F . For both adatoms the anisotropy of the vacuum LDOS shows only little magnetization-direction dependent differences in the unoccupied regions and giant values in the TMR effect are restricted to areas below E_F .

A closer look at the orbitally resolved LDOS of the adatoms in Fig. 4(c) and Fig. 5(c) reveals that the above-mentioned changes between both magnetization components in the vacuum can be attributed to p_z states of the adatoms which are mostly below E_F . The curves in the vacuum almost coincide with the ones for states of this character calculated directly at the respective adatom. As the p_z states are oriented along the surface normal, they preponderate in the vacuum compared to the p_x and p_y states. In contrast, the prominent peak of majority p_y states dominating the LDOS in the vicinity of E_F of both Pb and Bi is not visible in the vacuum LDOS because they are aligned parallel to the film plane. The shift of this peak, from a position of 0.2 eV above E_F for Pb, towards occupied regions for Bi can be explained by the increasing number of electrons in the p shell. On the other hand, the shift of the majority states with p_z character which are identified to generate the large anisotropy of the vacuum LDOS and hence the shift of the position of the maximum TMR can be ascribed to the different strength of the attractive potential acting between valence electrons and nucleus. Due to the larger nuclear charge these potentials lead to a stronger binding of the p_z states to the nucleus for Bi. Further reasons for the majority p_z states of the Bi adatom being shifted towards lower energies is the higher spin polarization compared to Pb as well as the smaller distance from its nearest neighbor Mn atom in the Mn monolayer. Hereby the orbital overlap increases resulting in a larger splitting of the states.

4. Modeling of the TMR

In order to explain the large TMR found for 6p adatoms adsorbed on Mn/W(110), we revert to the Hamiltonian of SOC mentioned in the introduction. As shown in Ref.⁴⁹, the SOC operator can be written as a matrix in the following way:

$$\mathcal{H}_{SOC} = \frac{\xi}{2} \begin{pmatrix} M & N \\ -N^* & M^* \end{pmatrix}. \quad (3)$$

Here, the diagonal matrices M describe the coupling of two states with equal spin direction, whereas the secondary diagonal matrices N denote the interaction of states with different spin character via SOC. Both can be calculated for an arbitrary orientation of the spin quantization axis by applying ladder operators of spin and angular momentum to linear combinations of complex spherical harmonics which represent both p and d orbitals. This approach yields the matrix element describing a spin-orbit induced hybridization between states with p_z and p_x symmetry in the same spin channel as⁵⁰:

$$\langle \uparrow, p_z | \mathcal{H}_{\text{SOC}} | p_x, \uparrow \rangle = i \sin \theta \sin \phi, \quad (4)$$

and the element for coupling states of the same symmetry, but with opposite spin direction as

$$\langle \uparrow, p_z | \mathcal{H}_{\text{SOC}} | p_x, \downarrow \rangle = \cos \phi + i \sin \phi \cos \theta. \quad (5)$$

In the first case (cf. Eq. (4)) the matrix element vanishes for the perpendicular magnetization direction ($\phi=0^\circ$, $\theta=0^\circ$) and becomes maximal for its magnetization pointing along the $[1\bar{1}0]$ direction ($\phi=90^\circ$, $\theta=90^\circ$), i.e. we expect a mixing of the two states only for a spin-quantization axis chosen along the film plane. The reverse is true if both states have opposite spin direction (cf. Eq. (5)). Evaluating the matrix elements given in Ref.⁵⁰ for a potential hybridization mediated by SOC for states with p_z and p_y character shows that such interaction can not be realized on the Mn/W(110) surface for the two above mentioned magnetization directions, which are possible on the substrate due to the spin spiral ground state. For this reason the discussion concerning the anisotropy of the vacuum LDOS is restricted to p_x and p_z states for both $6p$ adatoms and dimers in this paper.

Applying the above considerations first to the case of a Bi adatom on Mn/W(110) [Fig. 5], one can explain the maximum value of the TAMR at -0.57 eV below E_F by a magnetization-direction dependent mixing of p_x and p_z orbitals of opposite spin channels. At this energy the prominent peak of majority p_z states whose in-plane magnetization component resembles a single peak is split and shifted towards lower energies upon rotation of the spin-quantization axis (see Fig. 5(c)). According to the matrix elements, this behavior hints at a SOC-mediated hybridization with a minority p_x state which can be found at -0.82 eV.

The TAMR of the Pb adatom can also be understood based on the matrix elements of \mathcal{H}_{SOC} . E.g. the vacuum LDOS of the minority spin channel [Fig. 4(a)] just below E_F is reduced upon rotating the magnetization direction from in-plane to out-of-plane. This is due to mixing by SOC in the minority spin channel [Fig. 4(c)] between a p_z state located at -0.12 eV and a peak at -0.05 eV of p_x orbital character. For an in-plane magnetization direction, which allows mixing within the same spin channel by SOC according to Eq. (4), the p_x minority state peak at -0.05 eV splits into two peaks which coincide with the

positions of two minority states p_z peaks. This creates a large negative TAMR within the minority spin channel of -56% (not shown here). However, the TAMR is obtained from the total, spin-averaged LDOS. Just below the Fermi energy it is positive with a value of $+22\%$ due to a majority p_z peak whose height is reduced due to SOC for an in-plane magnetization [Fig. 4(c)]. The maximum TAMR effect of the Pb adatom of -49% occurs at 0.37 eV below E_F . It originates from the majority spin channel [Fig. 4(a)] and it is due to the splitting of a majority p_z state as can be seen from the orbital decomposition at the Pb atom [Fig. 4(c)]. Since the mixing occurs for a magnetization direction perpendicular to the surface it can be explained by a SOC induced mixing with p_x states of the opposite spin channel according to Eq. (5). While changes in the minority p_x LDOS can be noted within the relevant energy interval it is not possible to unambiguously propose a single peak which is responsible for the mixing. As will be discussed in detail for the Pb dimers at the end of this manuscript, there is also an impact of the Mn $3d$ states which are also subject to SOC and with which the Pb p states are hybridizing.

B. Pb and Bi dimers on Mn/W(110)

1. Structural and magnetic properties

Table III. The dimer bond lengths d (in Å) and the individual magnetic moments (in μ_B) of the adsorbed Pb and Bi dimers on the Mn monolayer on W(110). For comparison, the bond lengths and the magnetic moments of the free dimers (calculated with SOC) are given.

Orientation	Pb		Bi	
	d	μ_B	d	μ_B
[001]	3.23	+0.08	3.22	+0.12
[1 $\bar{1}$ 0]	3.35	+0.18	3.93	+0.02
[1 $\bar{1}$ 1]	3.11	± 0.02	3.12	± 0.02
Free	2.96	0.67	2.68	0.0

Since the Pb and Bi adatoms adsorb in the hollow-site position of the Mn layer, the dimers can be oriented along the [001], [1 $\bar{1}$ 0], and [1 $\bar{1}$ 1] directions (see Fig. 1(c)). The relaxed dimer bond lengths and the magnetic moments for the three orientations along with the values for free dimers are given in Table III. The dimer bond lengths increase after the adsorption due to structural relaxation from the bond length values of free dimers. For Pb dimers an increase of $\approx 10\%$ in bond length can be observed. For Bi dimers, a larger increase of $\approx 20\%$ in bond length has been observed except along the [1 $\bar{1}$ 0] orientation. In this case, we find an increase of bond length values by $\approx 45\%$.

In Pb dimers, the individual atoms carry small induced magnetic moments for all three orientations due to the hybridization with the Mn monolayer. Among the three

orientations, the largest individual magnetic moment of $+0.18 \mu_B$ is observed for the $[1\bar{1}0]$ orientation. These induced moments for Pb dimers are in contrast with the single atom adsorption where Pb remains nonmagnetic. Similar to the single adatom adsorption, Bi dimers also pick up small induced magnetic moment for all orientations with the largest value of $+0.12 \mu_B$ along the $[001]$ direction. Similar to the single adatom adsorption, reduction of magnetic moments for both nn and nnn Mn adatoms have been observed here as well.

2. Electronic properties

We proceed by describing and comparing the electronic structure of the dimers with those presented for the single adatoms before explaining the anisotropy of the LDOS. It should be pointed out here that the notation of the p orbitals of the dimers refers to the global coordinate axes of the Mn/W(110) surface as shown in Fig. 1, i.e. no local system for the adsorbates rotated for different orientations has been used. Therefore, the p_x and p_y orbitals of both $[001]$ and $[1\bar{1}0]$ dimers are aligned along the $[001]$ and $[1\bar{1}0]$ direction, respectively. As a result, the orbitals responsible for the covalent bond are changing.

Fig. 6 shows the m_l decomposed p states of both Pb and Bi dimers on a large energy scale around E_F . We will exemplify the differences in the LDOS compared to the single adatoms by means of the Bi dimers; similar observations can be made for the respective Pb adsorbates. Compared with the Bi adatom (cf. Fig. 2(f)), the Bi dimer along the $[001]$ orientation exhibits the largest modifications in its p_x orbitals which are responsible for the covalent bond in this case hereby forming σ orbitals (cf. Fig. 6(b)). This becomes most evident in the minority channel just below E_F where the corresponding states of the single adatom are shifted by 1 eV to the left due to the orbital overlap of the two atoms of the dimer. In contrast, the p_y and p_z states only show minor differences compared to the Bi adatom; especially the large peak of majority p_y states dominating close to E_F of the adatom is also found for the $[001]$ dimer.

Owing to the large distance of 3.93 \AA between the two Bi atoms of the $[1\bar{1}0]$ dimer the overlap of their orbitals is small resulting in similar features as for the adatom (cf. Fig. 6(d)). The main change in its m_l resolved LDOS is the disappearance of the dominant majority p_y peak at E_F which can be attributed to the fact that these orbitals are forming σ bonds in this case. For the Bi $[1\bar{1}1]$ dimer, differences in the m_l decomposed LDOS (cf. Fig. 6(f)) are clearly discernible compared to the single adatom (cf. Fig. 2(f)). This observation can partly be ascribed to the small bond length of 3.12 \AA and hence a large orbital overlap and partly to the combination of p_x and p_y states forming σ bonds. Both orbitals are tilted with respect to the global coordinate axes of the substrate leading to a covalent bond of a mixture of the two states with different symmetry. The p_z states which are crucial for STM are

relatively weakly affected for all dimers.

3. TAMR effect of the Pb dimers on Mn/W(110)

In the following section we study the TAMR of Pb dimers on Mn/W(110) for the three different dimer orientation discussed before.

In Fig. 7(a) both the total and spin-resolved components of the vacuum LDOS of the Pb dimer oriented along the $[001]$ direction are plotted for the two different magnetization directions which can occur due to the spin spiral states of the Mn monolayer on W(110). Note, that the in-plane magnetization direction is perpendicular to the dimer axis in this case. Compared to the respective adatom (cf. Fig. 4), only small differences between n_\perp and n_\parallel can be observed in the occupied regions below E_F . The most striking features occur now at energies -0.7 eV , -0.42 eV , -0.2 eV , and 0.05 eV leading to maximum values in the TAMR of $\pm 28\%$ (see Fig. 7(b)). Unlike the Pb adatom, the anisotropy of the vacuum LDOS takes another local maximum of $+29\%$ just above E_F . As one can see from the spin-resolved curves in Fig. 7(a), the TAMR at -0.7 eV stems from a modification of both spin channels upon rotation of the magnetization direction, whereas at E_F only majority states contribute whose perpendicular magnetization components are clearly enhanced compared to the parallel ones. Similar to the Pb adatom, differences between n_\perp and n_\parallel in the unoccupied regions are barely noticeable for both spin directions of the $[001]$ dimer.

The orbitally decomposed LDOS of this dimer plotted in Fig. 7(c), shows further similarities with the adatom. It is dominated by a prominent peak of majority p_y states at 0.15 eV above E_F which is not reflected in the vacuum LDOS and exhibits discernible changes in the p_z states with respect to both magnetization directions below E_F . The p_z states predominate the vacuum LDOS due to their double-lobed orbitals pointing along the surface normal. However, they experience a small shift towards lower energies as well as a splitting which is a consequence of the interaction between both Pb atoms composing the dimer.

Compared to the $[001]$ Pb dimer, the anisotropy of the vacuum LDOS is much larger for the dimer oriented along the $[1\bar{1}0]$ direction representing the propagation direction of the spin spiral on Mn/W(110) (see Fig. 7(d)-(e)). For this dimer orientation the in-plane magnetization direction is along the dimer axis (cf. Fig. 1). As for the single adatom, the appearance of the LDOS in the vacuum below E_F is characterized by magnetization-direction dependent differences of the majority p_z states where the main contribution comes from a dominant peak of the in-plane magnetized dimer at -0.45 eV below E_F . Being split multiple times upon reorientation of the spin-quantization axis, it creates a steep descent in the TAMR up to -64% thereby even exceeding the maximum value of the Pb adatom by 15% . Just above E_F , the anisotropy

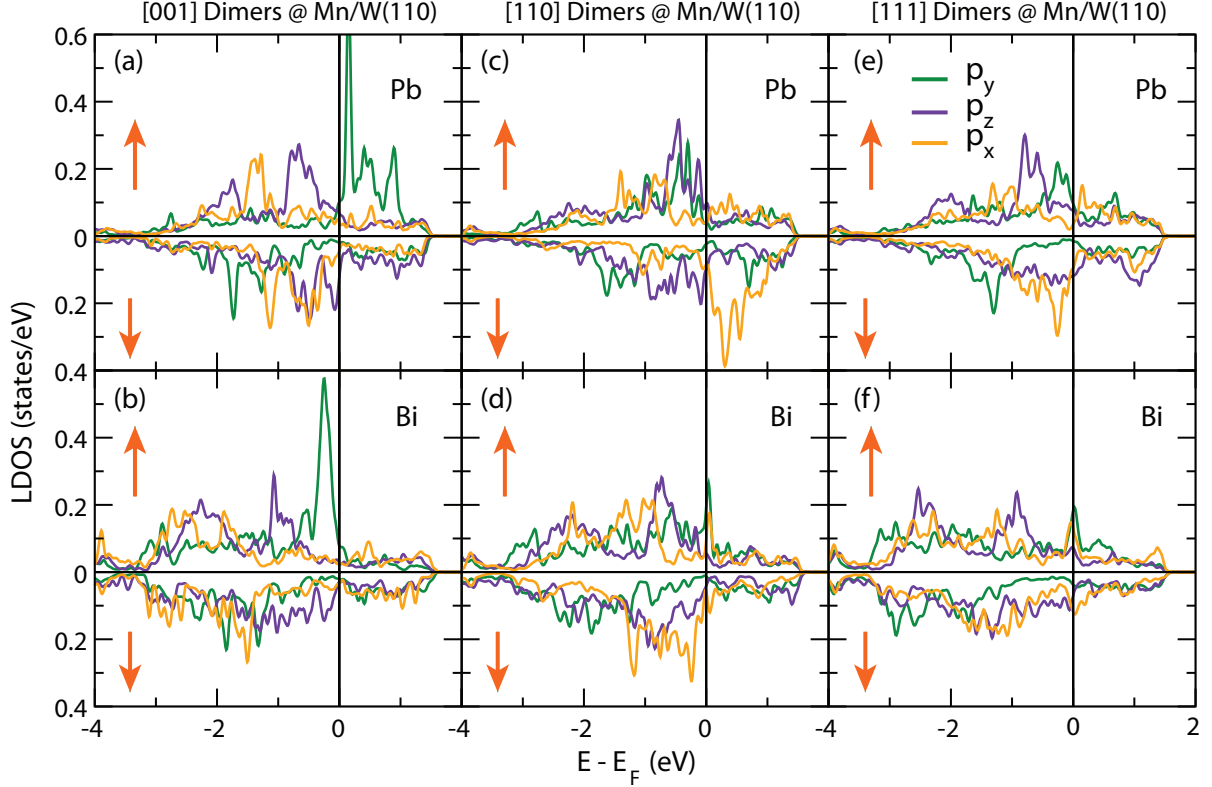


Figure 6. (a) Scalar relativistic spin and m_l resolved LDOS of the Pb and Bi dimers adsorbed on Mn/W(110) for (a, b) the [001] orientation, (c, d) $[1\bar{1}0]$ orientation, and (e, f) $[1\bar{1}1]$ orientation. The orange up and down arrow indicates majority and minority spin channels, respectively.

of the vacuum LDOS takes a local minimum of -38% which is due to the shift of a minority p_z state as the magnetization rotates from the perpendicular direction to the film plane along the $[1\bar{1}0]$ direction. The substantial similarity of the LDOS of this dimer in the p_z orbitals compared to the single adatom (cf. Fig. 4) can be explained by means of the relatively large distance of both Pb atoms (see Table III). If they are further apart, their interaction, i.e. the overlap of their orbitals, will be small thereby causing a similar behavior as for a single atom (cf. Fig. 4(c) and Fig. 7(f)). The p_y orbitals, on the other hand, which are forming σ bonds in the case of the $[1\bar{1}0]$ dimer are expected to show more remarkable differences in comparison with the adatom. This becomes mostly evident in the unoccupied regions where the prominent peak of majority p_y states is completely absent as seen in Fig. 7(f) with respect to the adatom (cf. Fig. 4(c)).

The electronic structure of the Pb dimer along $[1\bar{1}1]$ direction is shown in Fig. 7(g)-(i) for both magnetization directions. As for the [001] Pb dimer, only minor differences between n_\perp and n_\parallel are visible in the vacuum LDOS

above the $[1\bar{1}1]$ dimer along the diagonal of the unit cell. At -0.6 eV below E_F , a peak of majority states for parallel magnetization direction is enhanced compared to the perpendicular magnetization direction resulting in a negative TAMR of -25% . The vacuum LDOS of the unoccupied spectrum on the other hand is mainly characterized by magnetization-direction dependent changes of the minority states causing maximum values of $+28\%$ in the TAMR at $+0.62$ eV.

The magnitude of TAMR is much smaller for $[1\bar{1}1]$ dimer orientation as compared to the $[1\bar{1}0]$, which is oriented along the natural magnetization direction of the Mn/W(110) substrate. However, it is very similar as for the dimer oriented along [001], which is perpendicular to the magnetization of the surface. We will discuss these behavior in more detail in Section III B 5.

4. TAMR of Bi dimers on Mn/W(110)

Similar changes of the TAMR with the dimer orientation can be observed for Bi dimers on Mn/W(110). Con-

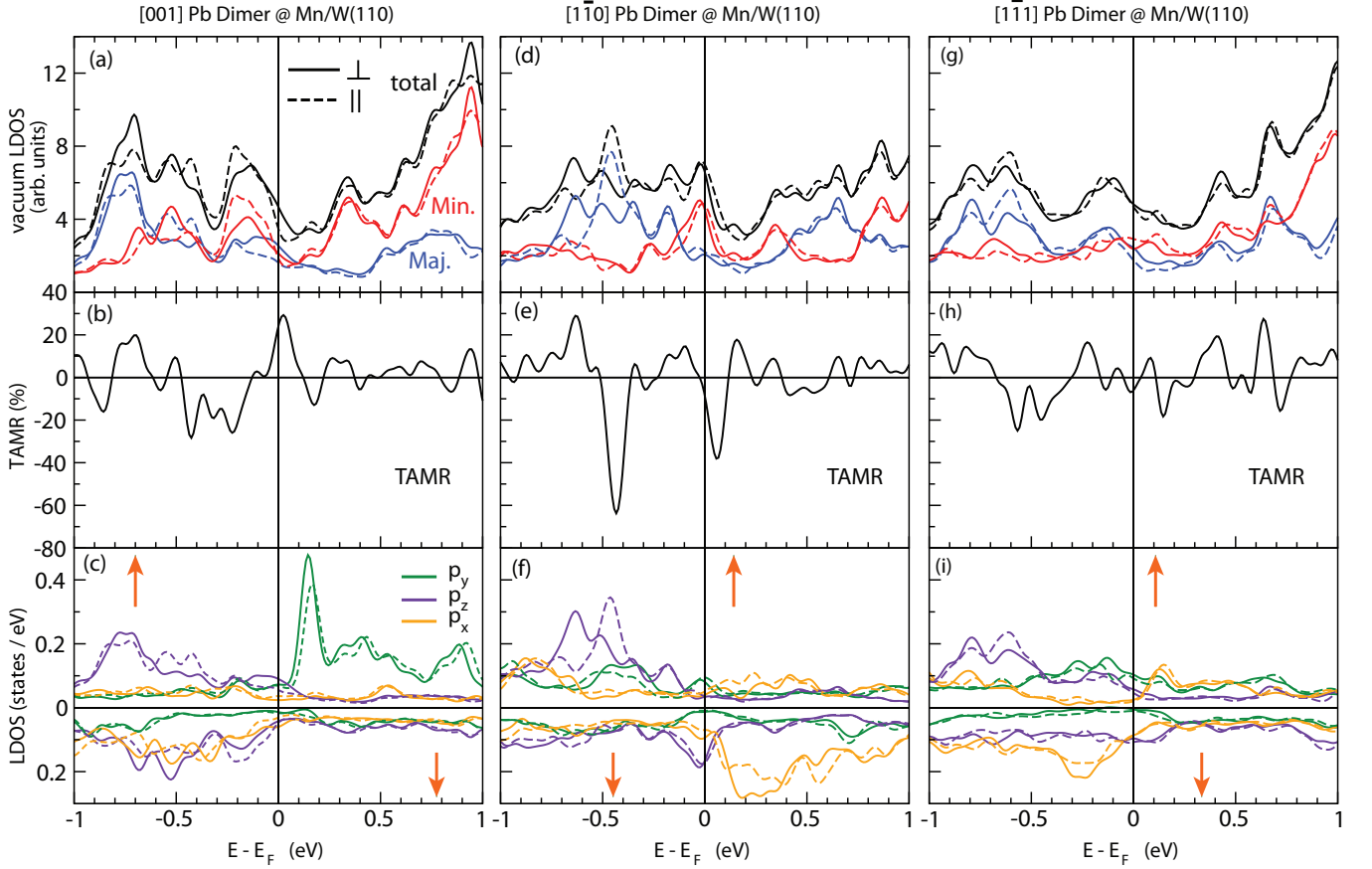


Figure 7. (a, d, g) Total (black lines) and spin-resolved (Majority: blue, Minority: red) vacuum LDOS above the Pb dimer on Mn/W(110) for out-of-plane (\perp , solid lines) and in-plane (parallel to the $[1\bar{1}0]$ direction) magnetizations (\parallel , dashed lines). (b, e, h) TMR obtained from the spin-averaged vacuum LDOS according to Eq. (2). (c, f, i) Orbital decomposition of the LDOS of the Pb dimers in terms of the majority (up) and minority (down) states. Solid (dashed) lines correspond to the magnetization direction perpendicular (parallel) to the surface plane. The orange up and down arrow indicates majority and minority spin channels, respectively.

Considering first the electronic structure of the $[001]$ Bi dimer which is shown in Fig. 8(a)-(c), one notices that as for the $[001]$ Pb dimer the curves for both magnetization directions of the spin-averaged vacuum LDOS do not differ significantly from each other. The largest differences are now located in the energy range between -0.9 and -0.3 eV leading to a local maximum in the TMR of -37% at -0.75 eV. The negative TMR value is much smaller than for the Bi adatom (cf. Fig. 5(b)). Consistent with the single Bi adatom, the energy range just below E_F is dominated by a large peak of minority states with p_z character (see Fig. 8(c)), whereas the prominent peak of majority p_y orbitals is absent in the vacuum LDOS due to its orientation within the film plane.

In contrast to the anisotropy of the vacuum LDOS of the corresponding Pb dimer, changes between n_\perp and n_\parallel vanish in the case of the $[001]$ Bi dimer directly at E_F . A closer look at the orbitally resolved LDOS reveals that the p_z states which dominate the LDOS above the surface are affected by the mutual interaction of both Bi atoms composing the dimer. In comparison with the

single Bi adatom, they are shifted towards lower energies and experience a larger splitting which is mostly apparent in the majority channel. The dominant peak of majority p_z states causing the large TMR of -61% at -0.57 eV for the single Bi adatom (cf. Fig. 5(b)) is therefore located outside of the presented energy range for the dimers. However, owing to the interaction of the orbitals it is split as well and less pronounced than for the single Bi adatom (not shown).

The hybridization of majority p_z orbitals is less prominent in the case of a Bi dimer oriented along the $[1\bar{1}0]$ direction (Fig. 8(d)-(f)) of the Mn/W(110) surface due to the large distance of nearly 4 Å between both Bi atoms. As one can see from its orbital decomposition in Fig. 8(f), p_z states move closer to E_F showing similar characteristics as in the case of the single Bi adatom (cf. Fig. 5). At $E_F - 0.55$ eV a dominant peak of majority p_z states for the in-plane magnetization orientation becomes visible which both decreases in height and shifts towards lower energies upon rotation of the spin-quantization axis. This is also the largest observable change between n_\perp and n_\parallel

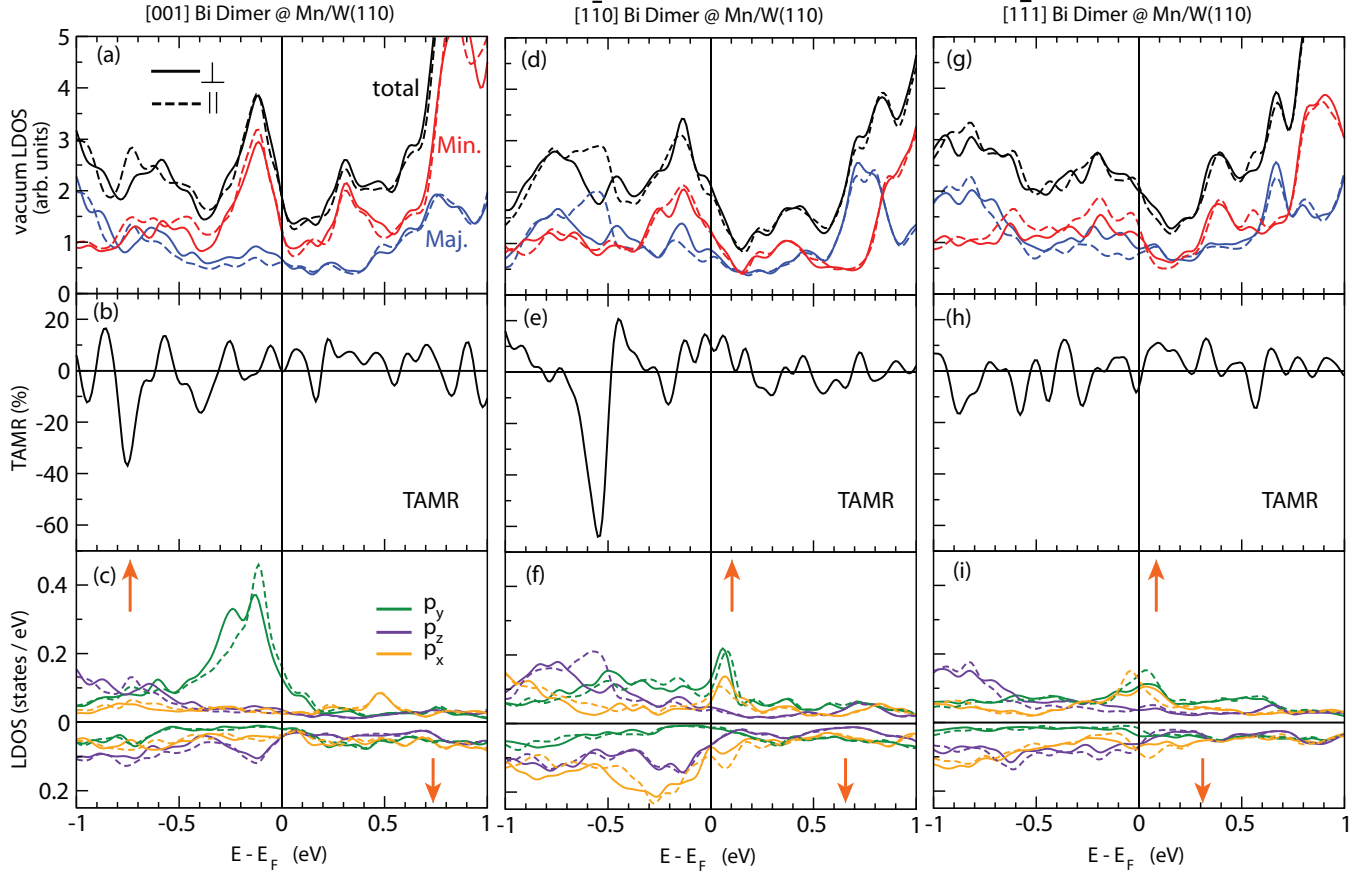


Figure 8. (a, d, g) Total (black lines) and spin-resolved (Majority: blue, Minority: red) vacuum LDOS above the Bi dimer on Mn/W(110) for out-of-plane (\perp , solid lines) and in-plane (parallel to the $[1\bar{1}0]$ direction) magnetizations (\parallel , dashed lines). (b, e, h) TAMR obtained from the spin-averaged vacuum LDOS according to Eq. (2). (c, f, i) Orbital decomposition of the LDOS of the Pb dimers in terms of the majority (up) and minority (down) states. Solid (dashed) lines correspond to the magnetization direction perpendicular (parallel) to the surface plane. The orange up and down arrow indicates majority and minority spin channels, respectively.

of the total (spin-averaged) vacuum LDOS for the $[1\bar{1}0]$ Bi dimer that is plotted in Fig. 8(d). The just mentioned magnetization-direction dependent changes in the majority p_z states thereby correspond to a huge TAMR effect of -64% at -0.55 eV. Hence, the anisotropy of the LDOS is in the same order of magnitude as for the single Bi adatom and takes its largest value at the same energetic position as well. The TAMR is considerably smaller for the rest of the presented energy range, especially at E_F where differences for parallel and perpendicular magnetizations of both spin channels only create a modest TAMR of approximately 15%.

As observed for the corresponding Pb dimer, only minor differences between both magnetization directions occur in the spin-averaged vacuum LDOS of the Bi dimer placed along the diagonal of the unit cell, i.e. the $[1\bar{1}1]$ direction. Whereas the spin-resolved curves are indeed clearly characterized by changes upon rotation of the magnetization in the occupied regions (see Fig. 8(g)), changes in the sum of both spin channels only lead to small values in the TAMR ranging from -16% at -0.8

eV up to -10% at E_F . As shown in the orbital decomposed LDOS of the dimer in Fig. 8(i), the main part of the anisotropy is created by the p_z orbitals. Additionally, this dimer orientation exhibits the smallest TAMR of all studied Bi dimer geometries and consistent with the previously presented results for $[1\bar{1}1]$ Pb dimers on Mn/W(110).

5. Origin of the TAMR for 6p dimers on Mn/W(110)

The variation of the TAMR magnitude depending on the orientation of both Pb and Bi dimers can partially be explained by means of a physical model considering two atomic states coupled via SOC proposed in Ref. 24. For a possible SOC induced hybridization of the dimer p states, we refer to the matrix elements presented in section III A 3. The orbitals are defined with respect to the global coordination axes of the unit cell.

Within this simplified model, our expectations match quite well with the 6p dimers oriented along the $[1\bar{1}0]$

direction showing the largest TAMR of all studied configurations. However, the SOC induced hybridization is not so clearly visible between their p_z and p_x states forming π_z and π_x molecular orbitals, respectively. The reduction of the TAMR effect for the $[1\bar{1}1]$ $6p$ dimers can be understood as well using the simplified model of two atomic states with differing orbital symmetry. For the case of a dimer orientation along the diagonal of the supercell the magnetization direction of the substrate is rotated with respect to the bonding axis of the atoms leading to a reduction of the respective matrix elements. For instance the hybridization between the p states, $\langle \uparrow, p_z | \mathcal{H}_{SOC} | p_x, \uparrow \rangle \propto \sin \theta \sin \phi$, is reduced for an azimuth angle of 45° . Since changes in the LDOS scale with the square of the matrix elements⁸, for both $6p$ dimers, the TAMR in $[1\bar{1}1]$ orientation is diminished by a factor of 4 compared to the $[1\bar{1}0]$ dimer ($\sim 15\%$ vs. $\sim 60\%$; cf. Fig. 7(e), Fig. 7(h) and Fig. 8(e), Fig. 8(h)). The same behavior has recently been observed for Pb dimers on a Fe bilayer on W(110)³⁰.

In addition, the p_x states are partially involved in the formation of molecular σ bonds along the dimer axis and thereby not available for the mixing with the p_z states which further reduces the possible value of the TAMR. The reduction of the LDOS of p_x states in the shown energy range due to hybridization is even more apparent in the $[001]$ and $[1\bar{1}1]$ Bi dimers (cf. Fig. 8(c), Fig. 8(i)) while it is similar to that of the Bi adatom (cf. Fig. 5) for the $[1\bar{1}0]$ dimer (cf. Fig. 8(f)).

For the $[001]$ Pb dimer, within the simplified model, one can interpret the changes in the curves of the minority p_x and p_z states upon rotation of the spin-quantization axis at -0.52 eV due to hybridization mediated by SOC (see Fig. 7(c)). The same effect could already be observed for the single Pb adatom directly at E_F (cf. Fig. 4(c)). If the dimer orientation ($[001]$) is perpendicular to the magnetization direction ($[1\bar{1}0]$) of the substrate, one would expect SOC to mix molecular π_z and antibonding σ^* orbitals which are composed of p_x states here³⁰. Molecular orbitals of this symmetry are located further apart in the energy spectrum than π_z and π_x molecular orbitals that can easily hybridize via SOC for a dimer axis along the magnetization of the Mn/W(110) surface, i.e., the $[1\bar{1}0]$ direction. Hence, within this simple model, the $[001]$ $6p$ dimers were expected to exhibit a much smaller variation of their electronic structure under the influence of SOC. However, our DFT calculations show that the anisotropy of the LDOS actually takes an unexpected high value of -28% and -37% for the case of the $[001]$ Pb and Bi dimer adsorbed on Mn/W(110), respectively. Hence, this model based on only two atomic/molecular states is not sufficient to quantitatively understand the TAMR for dimers along the $[001]$ axis.

In order to achieve a deeper understanding of the effect of $p-d$ hybridization on TAMR for the Pb and Bi dimers on Mn/W(110), we have calculated the partial charge densities within the scalar-relativistic approxima-

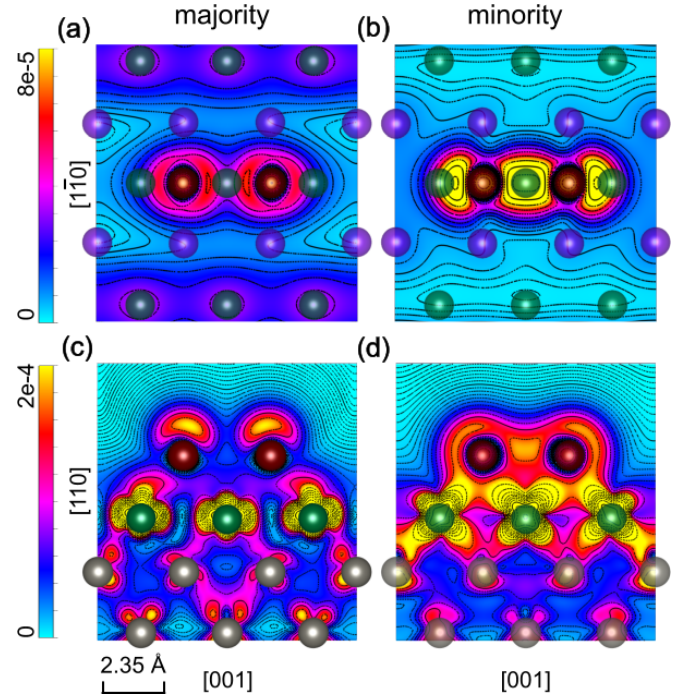


Figure 9. (a) and (b): top view (cross section) of the spin-resolved partial charge density plots of the Pb $[001]$ dimer on Mn/W(110) in the energy range $[E_F - 0.51, E_F - 0.49]$ eV. (c) and (d): cross-sectional plots through the Pb dimer parallel to the $[001]$ direction for the charge densities shown in (a) and (b).

tion, i.e., neglecting SOC, for a small energy range where the TAMR appears most prominent. The inclusion of SOC will not affect the hybridization as evident from the LDOS in the scalar relativistic approximation [Fig. 6] and including SOC [Figs. 7, 8]. In the following we exemplify the influence of the substrate by means of both $[001]$ and $[1\bar{1}0]$ Pb dimers only as we observe similar characteristic behaviors for the Bi dimers.

The spin-resolved partial charge density of the $[001]$ Pb dimer at approximately $E_F - 0.5$ eV at which the large TAMR of $\sim 28\%$ occurs (cf. Fig. 7(b)) is shown in Fig. 9. From the top view [Fig. 9(a,b)] which represents a cross section through the dimer one can clearly see the molecular π_z and σ_x character of the adsorbate for both spin channels, whereas from the side view [Fig. 9(c,d)] a strong hybridization with the d orbitals of the Mn atoms of the surface becomes visible. In the majority spin channel the axes of the p_z orbitals at the Pb dimer deviate from the z direction of the unit cell and the d orbitals of the Mn atoms are twisted towards the adsorbate [Fig. 9(c)]. This leads to a tilt of the upper lobes of the p_z orbitals towards the center of the dimer and an overlap of the lower lobes with the Mn d states in the case of the majority channel.

For the minority channel on the other hand [Fig. 9(d)] a clear differentiation between the Pb and Mn states is not possible anymore due to the strong hybridization which becomes manifest in an accumulation of the charge den-

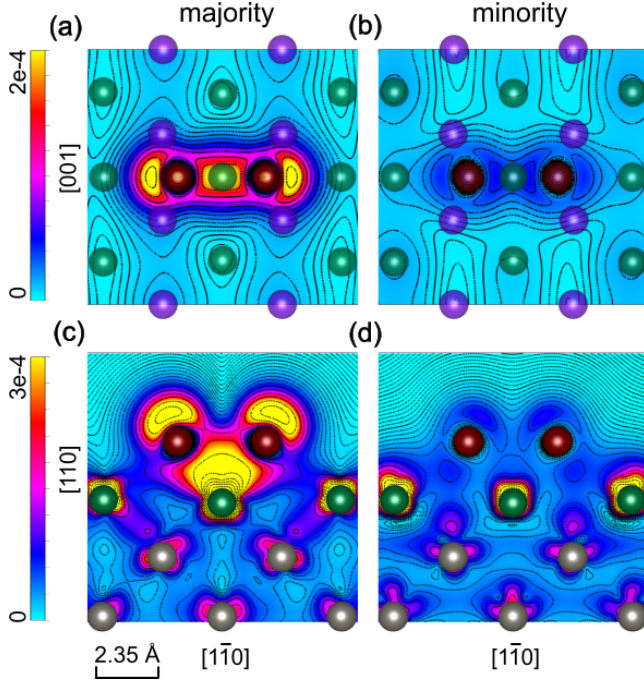


Figure 10. (a) and (b): top view (cross section) of the spin-resolved partial charge density plots of the Pb $[1\bar{1}0]$ dimer on Mn/W(110) in the energy range $[E_F - 0.46, E_F - 0.44]$ eV. (c) and (d): cross-sectional plots through the Pb dimer parallel to the $[1\bar{1}0]$ direction for the charge densities shown in (a) and (b).

sity at the interface. These observations already indicate that for the explanation of the TAMR effect of the $6p$ dimers on Mn/W(110) more than two atomic states have to be taken into account.

Hybrid Pb-Mn interface states are also present in the majority channel of the $[1\bar{1}0]$ Pb dimer at the position of the maximum TAMR around 0.45 eV below E_F (see Fig. 10). A closer look at the calculated charge density reveals that its majority p_z orbitals only interact with the Mn atom below the dimer axis, but not with the other atoms of the Mn monolayer [Fig. 10(c)]. Exactly the same behavior can also be observed for the corresponding $[1\bar{1}0]$ Bi dimer on Mn/W(110) (not shown). The reason for this hybridization can be explained by means of the different distances of the $6p$ atoms and their neighboring Mn atoms. While the central Mn atom and one atom of the Pb dimer are separated by just 2.84 Å, the respective distance towards the next Mn atoms is 3.15 Å and hence significantly larger.

However, the interaction with the central Mn atom described above cannot be realized for the $[1\bar{1}1]$ dimer since the respective atom of the substrate is missing below a bonding axis along the diagonal (see Fig. 1(c)).

Keeping in mind the studies of the partial charge densities, we did a further investigation of the LDOS of the central Mn atoms below the Pb dimer axes for the case of the $[001]$ and $[1\bar{1}0]$ direction. Fig. 11 shows their or-

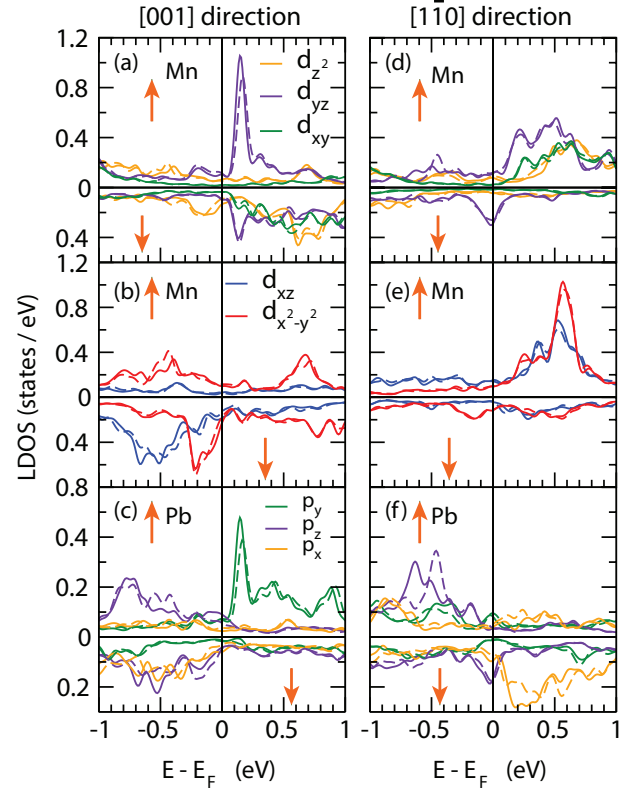


Figure 11. Orbital decomposed LDOS including SOC of the central Mn atoms below the $[001]$ and $[1\bar{1}0]$ Pb dimer in terms of the majority (up) and minority (down) states. Solid (dashed) lines correspond to the magnetization direction perpendicular (parallel) to the surface plane. The orange up and down arrow indicates majority and minority spin channels, respectively.

bitally decomposed d states in an energy interval of ± 1 eV around E_F along with the p states of the adsorbates for the two different magnetization directions discussed before. It is evident that the Mn atoms below both Pb dimers are likewise affected by the rotation of the magnetization direction and bear resemblance to the changes in the states of the Pb atoms at same energetic positions.

For the $[001]$ direction this becomes mostly apparent at 0.15 eV where a large peak of majority d_{yz} orbitals of the central Mn atom shows the same behavior upon a change of the spin-quantization axis as the dominant p_y state of the adsorbed dimer (cf. Fig. 7(c)). Moreover one can observe an enhancement of the parallel magnetization component of majority states with d_{z^2} and $d_{x^2-y^2}$ character at -0.41 eV which corresponds with a small peak of n_{\parallel} for the majority p_z states at the same energy. Further resemblance regarding magnetization-direction dependent differences in the LDOS are found between -0.70 eV and -0.50 eV for the minority d_{xz} orbitals of Mn and p_z and p_x orbitals of the $[001]$ Pb dimer.

For the $[1\bar{1}0]$ Pb dimer this SOC-dependent hybridization is most prominent for the d_{yz} states both at E_F in the minority channel and at $E_F - 0.45$ eV in the majority

channel. Especially at the last-mentioned position, for the in-plane magnetization, it becomes clear that the majority Mn d_{yz} states and the majority Pb p_z states interact quite strongly [Fig. 11] and produce a large TAMR value (see Fig. 7(e)).

IV. CONCLUSION

In conclusion, we have presented a detailed study of the spin-resolved electronic structure of single Pb and Bi adatoms and dimers adsorbed on the Mn monolayer on W(110) including the effect of spin-orbit coupling. Using density functional theory, we calculated the tunneling anisotropic magnetoresistance effect from two magnetization directions, imposed due to the cycloidal spin spiral ground state in the Mn layer, for the respective $6p$ adsorbate: perpendicular to the surface (out-of-plane) and parallel to the $[1\bar{1}0]$ direction representing the propagation direction of the spin spiral ground state (in-plane). Our calculations for the $6p$ adatoms which are characterized by large spin-orbit coupling constants predict an enhancement of the TAMR up to 49% for Pb and 61% for Bi adatoms.

In both cases it can mainly be attributed to magnetization-direction dependent changes of majority p_z states of the adatom. The anisotropy of the LDOS of both adatoms can generally be explained by means of a simplified physical model which considers the coupling of two atomic states with different orbital symmetry (p_z and p_x in the present case) via spin-orbit coupling. Although Pb and Bi adatoms carry almost no magnetic moment, they exhibit a large spin polarization directly at the surface and also in the vacuum due to the hybridization with the substrate. The spin polarization becomes

maximal with values up to 60% around E_F for the Pb adatom.

We have also investigated the TAMR for three different dimer orientations adsorbed on the Mn/W(110) surface. Consistent with the expectations both Pb and Bi dimers with their bonding axis along the magnetization direction of the substrate, i.e. the $[1\bar{1}0]$ direction, show the maximum anisotropy of the vacuum LDOS with values of 64% in the occupied regions. The origin of this large effect is a molecular π_z orbital with majority spin character which strongly interacts with the central Mn atom below the dimer axis. Similar interactions are also found for a dimer orientation perpendicular to the magnetization direction of Mn/W(110), but with much smaller TAMR values of 37% for Bi and 28% for Pb, respectively. The TAMR becomes minimal for $6p$ dimers along the diagonal $[1\bar{1}1]$ direction (16% in the case of Bi, 27% for Pb) due to reduced SOC induced mixing of the p states on the one hand and due to missing Mn atoms for hybridization below their bonding axes on the other hand. A further exploration of the central Mn atoms below the $[001]$ and $[1\bar{1}0]$ dimers has shown that their d orbitals are likewise affected by changes upon rotation of the magnetization direction which has to be taken into account for the comprehension of the TAMR effect apart from the simple model of only two atomic states interacting by SOC.

ACKNOWLEDGMENTS

We acknowledge the DFG via SFB677 for financial support. We gratefully acknowledge the computing time at the supercomputer of the North-German Supercomputing Alliance (HLRN). We thank N. M. Caffrey for valuable discussions.

* Corresponding author: haldar@physik.uni-kiel.de
haldar.physics@gmail.com

¹ Y. Yayon, V. W. Brar, L. Senapati, S. C. Erwin, and M. F. Crommie, Observing spin polarization of individual magnetic adatoms, *Phys. Rev. Lett.* **99**, 067202 (2007).

² F. Meier, L. Zhou, J. Wiebe, and R. Wiesendanger, Revealing magnetic interactions from single-atom magnetization curves, *Science* **320**, 82 (2008).

³ K. Tao, V. S. Stepanyuk, W. Hergert, I. Rungger, S. Sanvito, and P. Bruno, Switching a single spin on metal surfaces by a stm tip: Ab initio studies, *Phys. Rev. Lett.* **103**, 057202 (2009).

⁴ S. Loth, K. von Bergmann, M. Ternes, A. F. Otte, C. P. Lutz, and A. J. Heinrich, Controlling the state of quantum spins with electric currents, *Nature Physics* **6**, 340 (2010).

⁵ M. Ziegler, N. Néel, C. Lazo, P. Ferriani, S. Heinze, J. Kröger, and R. Berndt, Spin valve effect in single-atom contacts, *New Journal of Physics* **13**, 085011 (2011).

⁶ C. Lazo, N. Néel, J. Kröger, R. Berndt, and S. Heinze, Tunneling magnetoresistance and exchange interaction in single-atom contacts, *Phys. Rev. B* **86**, 180406(R) (2012).

⁷ A. A. Khajetoorians, B. Baxevanis, C. Hübner, T. Schlenk, S. Krause, T. O. Wehling, S. Lounis, A. Lichtenstein, D. Pfannkuche, J. Wiebe, and R. Wiesendanger, Current-driven spin dynamics of artificially constructed quantum magnets, *Science* **339**, 55 (2013).

⁸ M. Bode, S. Heinze, A. Kubetzka, O. Pietzsch, X. Nie, G. Bihlmayer, S. Blügel, and R. Wiesendanger, Magnetization-direction-dependent local electronic structure probed by scanning tunneling spectroscopy, *Phys. Rev. Lett.* **89**, 237205 (2002).

⁹ C. Gould, C. Rüster, T. Jungwirth, E. Girgis, G. M. Schott, R. Giraud, K. Brunner, G. Schmidt, and L. W. Molenkamp, Tunneling anisotropic magnetoresistance: A spin-valve-like tunnel magnetoresistance using a single magnetic layer, *Phys. Rev. Lett.* **93**, 117203 (2004).

¹⁰ P. Gambardella, S. Rusponi, M. Veronese, S. S. Dhesi, C. Grazioli, A. Dallmeyer, I. Cabria, R. Zeller, P. H. Dederichs, K. Kern, C. Carbone, and H. Brune, Giant magnetic anisotropy of single cobalt atoms and nanoparticles, *Science* **300**, 1130 (2003).

- ¹¹ C. F. Hirjibehedin, C.-Y. Lin, A. F. Otte, M. Ternes, C. P. Lutz, B. A. Jones, and A. J. Heinrich, Large magnetic anisotropy of a single atomic spin embedded in a surface molecular network, *Science* **317**, 1199 (2007).
- ¹² S. Loth, M. Etzkorn, C. P. Lutz, D. M. Eigler, and A. J. Heinrich, Measurement of fast electron spin relaxation times with atomic resolution, *Science* **329**, 1628 (2010).
- ¹³ A. A. Khajetoorians, S. Lounis, B. Chilian, A. T. Costa, L. Zhou, D. L. Mills, J. Wiebe, and R. Wiesendanger, Itinerant nature of atom-magnetization excitation by tunneling electrons, *Phys. Rev. Lett.* **106**, 037205 (2011).
- ¹⁴ I. G. Rau, S. Baumann, S. Rusponi, F. Donati, S. Stepanow, L. Gragnaniello, J. Dreiser, C. Piamonteze, F. Nolting, S. Gangopadhyay, O. R. Albertini, R. M. Macfarlane, C. P. Lutz, B. A. Jones, P. Gambardella, A. J. Heinrich, and H. Brune, Reaching the magnetic anisotropy limit of a 3d metal atom, *Science* **344**, 988 (2014).
- ¹⁵ A. Fert, The present and the future of spintronics, *Thin Solid Films* **517**, 2 (2008).
- ¹⁶ J. Sinova and I. Žutić, New moves of the spintronics tango, *Nat. Mater.* **11**, 368 (2012).
- ¹⁷ A. B. Shick, F. Máca, J. Mašek, and T. Jungwirth, Prospect for room temperature tunneling anisotropic magnetoresistance effect: Density of states anisotropies in CoPt systems, *Phys. Rev. B* **73**, 024418 (2006).
- ¹⁸ A. N. Chantis, K. D. Belashchenko, E. Y. Tsymlal, and M. van Schilfgaarde, Tunneling anisotropic magnetoresistance driven by resonant surface states: First-principles calculations on an Fe(001) surface, *Phys. Rev. Lett.* **98**, 046601 (2007).
- ¹⁹ A. Matos-Abiad and J. Fabian, Anisotropic tunneling magnetoresistance and tunneling anisotropic magnetoresistance: Spin-orbit coupling in magnetic tunnel junctions, *Phys. Rev. B* **79**, 155303 (2009).
- ²⁰ A. Matos-Abiad, M. Gmitra, and J. Fabian, Angular dependence of the tunneling anisotropic magnetoresistance in magnetic tunnel junctions, *Phys. Rev. B* **80**, 045312 (2009).
- ²¹ L. Gao, X. Jiang, S.-H. Yang, J. D. Burton, E. Y. Tsymlal, and S. S. P. Parkin, Bias voltage dependence of tunneling anisotropic magnetoresistance in magnetic tunnel junctions with MgO and Al₂O₃ tunnel barriers, *Phys. Rev. Lett.* **99**, 226602 (2007).
- ²² M. Viret, M. Gabureac, F. Ott, C. Fermon, C. Barreteau, G. Autes, and R. Guirado-Lopez, Giant anisotropic magnetoresistance in ferromagnetic atomic contacts, *The European Physical Journal B - Condensed Matter and Complex Systems* **51**, 1 (2006).
- ²³ K. I. Bolotin, F. Kuemmeth, and D. C. Ralph, Anisotropic magnetoresistance and anisotropic tunneling magnetoresistance due to quantum interference in ferromagnetic metal break junctions, *Phys. Rev. Lett.* **97**, 127202 (2006).
- ²⁴ N. Néel, S. Schröder, N. Ruppelt, P. Ferriani, J. Kröger, R. Berndt, and S. Heinze, Tunneling anisotropic magnetoresistance at the single-atom limit, *Phys. Rev. Lett.* **110**, 037202 (2013).
- ²⁵ J. Schöneberg, F. Otte, N. Néel, A. Weismann, Y. Mokrousov, J. Kröger, R. Berndt, and S. Heinze, Ballistic anisotropic magnetoresistance of single-atom contacts, *Nano Letters* **16**, 1450 (2016).
- ²⁶ A. B. Shick, S. Khmelevskyi, O. N. Mryasov, J. Wunderlich, and T. Jungwirth, Spin-orbit coupling induced anisotropy effects in bimetallic antiferromagnets: A route towards antiferromagnetic spintronics, *Phys. Rev. B* **81**, 212409 (2010).
- ²⁷ B. G. Park, J. Wunderlich, X. Martí, V. Holý, Y. Kurosaki, M. Yamada, H. Yamamoto, A. Nishide, J. Hayakawa, H. Takahashi, A. B. Shick, and T. Jungwirth, A spin-valve-like magnetoresistance of an antiferromagnet-based tunnel junction, *Nature Materials* **10**, 347 (2011).
- ²⁸ M. Hervé, T. Balashov, A. Ernst, and W. Wulfhekel, Large tunneling anisotropic magnetoresistance mediated by surface states, *Phys. Rev. B* **97**, 220406(R) (2018).
- ²⁹ S. D. Borisova, G. G. Rusina, S. V. Eremeev, and E. V. Chulkov, Dimers of heavy p-elements of groups IV–VI: Electronic, vibrational, and magnetic properties, *JETP Lett.* **103**, 471 (2016).
- ³⁰ J. Schöneberg, P. Ferriani, S. Heinze, A. Weismann, and R. Berndt, Tunneling anisotropic magnetoresistance via molecular π orbitals of Pb dimers, *Phys. Rev. B* **97**, 041114(R) (2018).
- ³¹ A. Fert, V. Cros, and J. Sampaio, Skyrmions on the track, *Nat. Nano.* **8**, 152 (2013).
- ³² N. Nagaosa and Y. Tokura, Topological properties and dynamics of magnetic skyrmions, *Nat. Nano.* **8**, 899 (2013).
- ³³ M. Bode, M. Heide, K. von Bergmann, P. Ferriani, S. Heinze, G. Bihlmayer, A. Kubetzka, O. Pietzsch, S. Blügel, and R. Wiesendanger, Chiral magnetic order at surfaces driven by inversion asymmetry, *Nature* **447**, 190 (2007).
- ³⁴ D. Serrate, P. Ferriani, Y. Yoshida, S.-W. Hla, M. Menzel, K. von Bergmann, S. Heinze, A. Kubetzka, and R. Wiesendanger, Imaging and manipulating the spin direction of individual atoms, *Nature Nanotech.* **5**, 350 (2010).
- ³⁵ D. Serrate, Y. Yoshida, M. Moro-Lagares, A. Kubetzka, and R. Wiesendanger, Spin-sensitive shape asymmetry of adatoms on noncollinear magnetic substrates, *Phys. Rev. B* **93**, 125424 (2016).
- ³⁶ S. Haldar and S. Heinze, Noncollinear spin density of an adatom on a magnetic surface, *Phys. Rev. B* **98**, 220401(R) (2018).
- ³⁷ N. M. Caffrey, S. Schröder, P. Ferriani, and S. Heinze, Tunneling anisotropic magnetoresistance effect of single adatoms on a noncollinear magnetic surface, *Journal of Physics: Condensed Matter* **26**, 394010 (2014).
- ³⁸ S. Heinze, M. Bode, A. Kubetzka, O. Pietzsch, X. Nie, S. Blügel, and R. Wiesendanger, Real-space imaging of two-dimensional antiferromagnetism on the atomic scale, *Science* **288**, 1805 (2000).
- ³⁹ G. Kresse and J. Furthmüller, Efficient iterative schemes for *ab Initio* total-energy calculations using a plane-wave basis set, *Phys. Rev. B* **54**, 11169 (1996).
- ⁴⁰ See <https://www.vasp.at>.
- ⁴¹ P. E. Blöchl, Projector augmented-wave method, *Phys. Rev. B* **50**, 17953 (1994).
- ⁴² G. Kresse and D. Joubert, From ultrasoft pseudopotentials to the projector augmented-wave method, *Phys. Rev. B* **59**, 1758 (1999).
- ⁴³ J. P. Perdew, K. Burke, and M. Ernzerhof, Generalized gradient approximation made simple, *Phys. Rev. Lett.* **77**, 3865 (1996).
- ⁴⁴ J. P. Perdew, K. Burke, and M. Ernzerhof, Generalized gradient approximation made simple [phys. rev. lett. 77, 3865 (1996)], *Phys. Rev. Lett.* **78**, 1396 (1997).
- ⁴⁵ D. Hobbs, G. Kresse, and J. Hafner, Fully unconstrained noncollinear magnetism within the projector augmented-wave method, *Phys. Rev. B* **62**, 11556 (2000).

- ⁴⁶ H. J. Monkhorst and J. D. Pack, Special points for brillouin-zone integrations, Phys. Rev. B **13**, 5188 (1976).
- ⁴⁷ J. Tersoff and D. R. Hamann, Theory and application for the scanning tunneling microscope, Phys. Rev. Lett. **50**, 1998 (1983).
- ⁴⁸ J. Tersoff and D. R. Hamann, Theory of the scanning tunneling microscope, Phys. Rev. B **31**, 805 (1985).
- ⁴⁹ E. Abate and M. Asdente, Tight-binding calculation of 3d bands of fe with and without spin-orbit coupling, Phys. Rev. **185**, 861 (1969).
- ⁵⁰ J. Schöneberg, *Magnetoresistance of atomic structures studied with a Scanning Tunneling Microscope*, Ph.D. thesis, University of Kiel (2016).